Design of overvoltage suppression filter based on high-frequency modeling of cable in SiC based motor drive

Available online at www.sciencedirect.com
ScienceDirect
Energy Reports 8 (2022) 822–831
www.elsevier.com/locate/egyr

The 5th International Conference on Electrical Engineering and Green Energy, CEEGE 2022, 8-11 June, Berlin, Germany

Design of overvoltage suppression filter based on high-frequency modeling of cable in SiC based motor drive

Haihong Qin[a,*], Haoxiang Hu[a], Feifei Bu[a], Qian Xun[b], Wenming Chen[a], Dafeng Fu[a]

[a] *College of Automation Engineering, Nanjing University of Aeronautics and Astronautics, Nanjing 211106, China*
[b] *Division of Electric Power Engineering, Department of Electrical Engineering, Chalmers University of Technology, Hörsalsvägen 11, Gothenburg, SE-41279, Sweden*

Received 16 July 2022; accepted 5 August 2022
Available online xxxx

Abstract

SiC-based motor drives have the advantages of achieving higher efficiency and higher power density than traditional Si-based motor drives, and are gradually being widely used in electric power transmission. Due to different application situations such as oil field and airplane, a long cable is applied between the motor drive and three-phase motor and the distance may exceed hundreds of meters, which will cause serious voltage reflection problem, damaging working life of the motor. Meanwhile, the high slew rate of output voltage created by SiC-based motor drive deteriorates this phenomenon. In order to solve this problem, we first analyze the principle and influencing factors of voltage reflection, and establish the equivalent circuit model of the long cable. Then we put forward design method of *LRC* passive filter to suppress voltage reflection, and give simulation analysis. At last we built an experimental platform to verify the effectiveness of the *LRC* passive filter in SiC-based motor drive, and the experimental results show that the *LRC* passive filter with optimized parameters has good suppression effect of voltage reflection.

Peer-review under responsibility of the scientific committee of the 4th International Conference on Electrical Engineering and Green Energy, CEEGE, 2021.

Keywords: SiC; Voltage reflection; Long cable; *LRC* filter

1. Introduction

Wide-bandgap (WBG) semiconductors such as silicon carbide (SiC) have better electrical characteristics and thermal stability compared with silicon (Si) semiconductors [1]. So they are widely used in high frequency and high power applications due to their low power losses, fast switching speed, and high temperature capabilities. These advantages can effectively improve power density and switching frequency of the SiC-based motor drive system, which make them widely used in special applications such as aerospace and ship propulsion. However,

* Corresponding author.
E-mail address: qinhaihong@nuaa.edu.cn (H. Qin).

https://doi.org/10.1016/j.egyr.2022.08.025

Peer-review under responsibility of the scientific committee of the 4th International Conference on Electrical Engineering and Green Energy, CEEGE, 2021.

as new devices used in complex motor drive system, there still have many challenges to be solved to utilize their advantages completely [2].

In the fields of transportation including aerospace and ship propulsion, motors and drives often need to be connected with long cables due to their placement restrictions [3]. When a PWM pulse is launched to a long cable, part of it could reflect back to the motor drive at load terminals because the impedance of the long cable cannot match with the motor, which caused overvoltage phenomena at motor terminals. If the impedance of both ends of the motor matches, there will not exist voltage reflections. Meanwhile, the high dv/dt caused by high switching speed of SiC-based motor drive results in more serious voltage reflection phenomena [4].

An open-end winding ac motor drive configuration is exploited in [5], and the overvoltage generated by one inverter at motor terminals is effectively reduced by an adaptive pulse generated by the other one. This method is relying on coordinated operations of the two motor drives, and requires the special configuration of motor terminals, which is not applied widely. In [6], a PWM pulse pattern to calculate characteristic impedance and oscillation frequency of the long cable between the inverter and motor is developed. This method does not increase the size of the system and has the self-adjustment ability. However, the long dwell time in PWM pulse pattern may cause distortion of the output voltage waveform. A quasi-three-level PWM scheme is developed in [7], and this pattern adopts a brief zero-voltage state with a predetermined time. The results show that the overvoltage phenomenon is significantly discontinued after two propagation cycles, but the complexity of control algorithm and three-level inverter are limited the applicable scope. So we turned to filter design. An active reflected wave canceller (ARWC) to suppress overvoltage is presented in [8,9], and the power loss is extremely low with the PWM pulse pattern, which has same effect with passive filter. But the additional power devices increase the size and cost of the system. [10] presents a multi-domain design of dv/dt filters, which includes consideration of electrical, magnetic, and thermal domains. Compared with passive filters, its size and filtering effect are greatly improved, but the common current reduction is not considered for the method of design, and common current is significant for motor drives. A passive *LRC* filter design method is developed in [11], and the high-frequency modeling of the long cable is put forward. But the test method of the characteristic impedance of the cable was not given.

The purpose of this paper is to propose the extracting method the high-frequency parameters of the cable and present the design method of passive *LRC* filter, and verify the effectiveness of these methods in SiC-based motor drive platform.

In this paper, the principle of voltage reflection is analyzed, and we discuss the impact factors of the overvoltage at motor terminals, and produce the high-frequency model of the cable, which is established to extract accurate high-frequency parameters in Section 2. Thus the parameters needed by the design of LRC filter can be obtained. In Section 3, we analyze the mechanism of LRC filter and put forward the detailed design method of LRC passive filter to suppress voltage reflection. In Section 4, the experimental results are presented with the comparisons between the overvoltage phenomenon with LRC filter and the conventional one. Section 5 summarizes the main conclusions of this paper.

2. Analysis of voltage reflection on motor and high frequency cable modeling

2.1. Influencing factors of voltage reflection

In order to analyze the voltage reflection process in the real motor drive system, the dv/dt of the PWM pulse and the characteristics of the cable are taken into consideration. The transmission line is equivalent to a two-port network, and its equivalent circuit diagram is shown in Fig. 1. U_s is the amplitude of PWM pulse generated by the inverter, Z_s is the impedance of the inverter, Z_C is the characteristic impedance of the cable, Z_L is the impedance of motor, and l_{cable} is the length of the cable.

When the PWM pulse u^+ on the cable is transmitted to the motor terminal from the inverter, voltage reflection occurs at the motor, then a reflected wave u^- with an attenuated amplitude is generated. The reflection coefficient Γ_L at the motor can be described as (1), and the characteristic impedance Z_C of the cable can be described as (2):

$$\Gamma_L = \frac{(Z_L - Z_C)}{(Z_L + Z_C)} \tag{1}$$

$$Z_C = \sqrt{\frac{L_0}{C_0}} \tag{2}$$

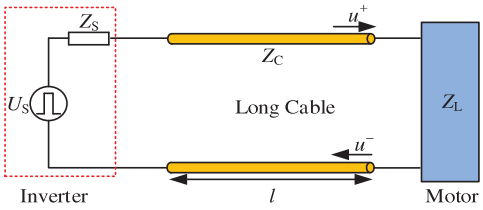

Fig. 1. Equivalent circuit of motor drive system with a long cable.

where L_0 is the equivalent inductance of a unit length cable; C_0 is the equivalent capacitance of a unit length cable. The reflection coefficient Γ_S at the inverter can also be described as $(Z_S - Z_C)/(Z_S + Z_C)$.

The actual transmission process of the pulse voltage on the cable is shown in Fig. 2(a). The number of the red circle represents the number of voltage reflection times. There is a large inductance Z_L on the stator winding of the motor, then $Z_L >> Z_C$, combined with formula (1), we can see that $\Gamma_L \approx 1$; while the inverter can be regarded as a voltage source with small internal resistance, then $Z_C >> Z_S$, so $\Gamma_S \approx -1$.

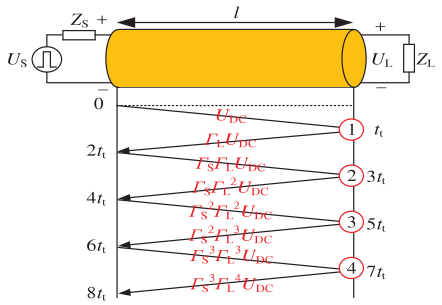

(a) Transmission process of PWM pulse when long cable is connected

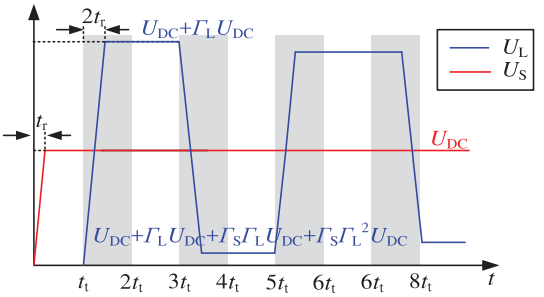

(b) Schematic diagram of motor terminal voltage change during voltage reflection

Fig. 2. The schematic diagram of voltage reflection process with consideration of the cable.

The schematic diagram of the voltage changes at the inverter end and the motor end during the whole process is shown in Fig. 2(b). According to the above analysis, the voltage reflection process in the actual motor drive system is as follows. The first reflection occurs at t_t, the transmitted reflected wave is the same as the incident wave, and the amplitude becomes $\Gamma_L U_{DC}$ ($\Gamma_L \approx 1$), so the reflection makes the motor terminal voltage $U_{DC} + \Gamma_L U_{DC}$, which is approximately twice. At $2t_t$, the inverter received the first reflected wave $\Gamma_L U_{DC}$. The voltage on the cable will drop since the reflected wave $\Gamma_S\Gamma_L U_{DC}$ will turn positive to negative. When the reflected wave $\Gamma_S\Gamma_L U_{DC}$ reaches back to the motor, the voltage basically returns to zero because $U_{DC} + \Gamma_L U_{DC} + \Gamma_S\Gamma_L\Gamma_S\Gamma_L U_{DC} + \Gamma_S\Gamma_L^2 U_{DC} \approx 0$. A complete oscillation cycle is finished at $4t_t$.

If the rise time t_r of PWM pulse is too long or the cable length l_{cable} is very short, the PWM pulse is still rising in the third transmission cycle, and the voltage at the motor terminal will decrease due to the negative reflected wave. The critical length l_{cable_c} is defined as:

$$l_{cable\_c} = v \cdot \frac{t_r}{3} \tag{3}$$

Peak voltage value of the motor can be described as follow when $t_t < t_r/3$.

$$U_{peak\_motor} = \frac{3lU_{DC}\Gamma_L}{vt_r} + U_{DC} \tag{4}$$

After normalization:

$$U_{peak\_motor}/U_{DC} = \frac{3l\Gamma_L}{vt_r} + 1 \tag{5}$$

$U_{\text{peak\_motor}}$ generally does not exceed 120% of U_{DC}. According to Eq. (5), the critical rise time $t_{\text{r\_c}}$ of the PWM pulse is obtained as:

$$t_{\text{r\_c}} = \frac{15l\Gamma_{\text{L}}}{v} \tag{6}$$

It can be seen from the above analysis that the main factors affecting the voltage reflection are the length of the cable and the rise time of the PWM pulse.

2.2. Modeling and extraction of high frequency impedance of long cables

The switching speed of the SiC MOSFET in motor drive system is within 100 ns, which will greatly increase the rise time of the PWM pulse and generate a large amount of high-frequency components. According to the transmission line theory, when a high-frequency signal passes through a long cable, the wave length of the signal will change, and the influence of the distribution parameters such as inductance, and capacitance on the cable cannot be ignored. Therefore, it is necessary to establish a high-frequency equivalent model of the long cables.

The equivalent model of the long cable is established as shown in Fig. 3. A single wire can be equivalent to a resistor R_0 and an inductance L_0 in series, and when there are multiple wires, a coupling effect will occur between them, that is, there will be a capacitance C_0 and a conductance G_0.

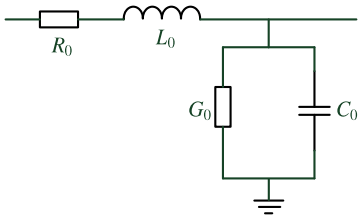

Fig. 3. The equivalent model of the long cable.

In order to accurately extract the high-frequency impedance of the cable, we take the 9 m AWG10 cable used in the experiment as an example, and utilize the network analyzer E5016B as test instrument, and the measurement frequency band is selected as 100 kHz–4 MHz. The short-circuit impedance Z_{SC} and open-circuit impedance Z_{OC} of the cable are measured. The measurement methods are shown in Fig. 4.

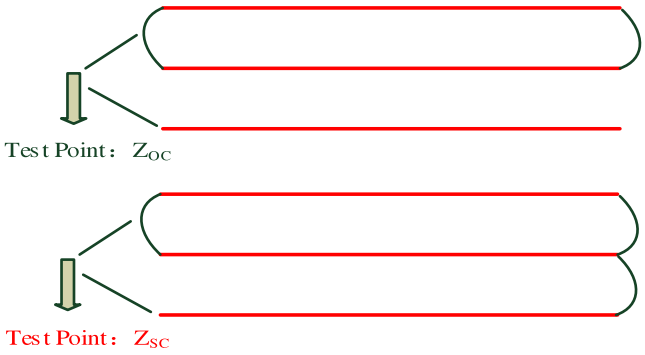

Fig. 4. Schematic diagram of measurement methods of Z_{SC} and Z_{OC}.

The measurement results of the cable are shown in Fig. 5.

For short-circuit impedance Z_{SC}, the equivalent resistance R_0 of the cable can be measured by the measuring instrument (LCR) at a low frequency of 100 Hz, and the result of R_0 is 64 mΩ. The equivalent inductance L_0 should be tested at a high frequency (3 MHz), and the results of Z_{SC} is 127.07 Ω, the short-circuit angle is 89°, so L_0 is 4.49 μH. For open-circuit impedance Z_{OC}, the value can be described by the first resonant frequency 4.48 MHz, so

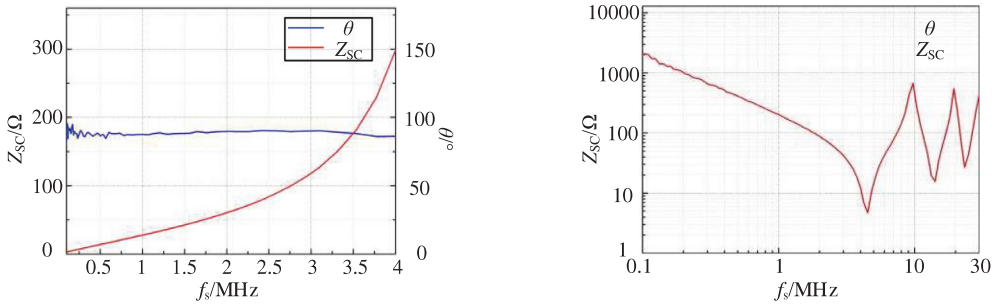

（a）Measurement results of Z_{SC} （b）Measurement results of Z_{OC}

Fig. 5. Measurement results of the cable.

the value of equivalent capacitance C_0 is 281 pF. Due to the higher insulation level of the cable, the conductance G_0 is negligible, the results of high-frequency parameters per unit length of AWG10 are given in Table 1.

Table 1. High-frequency parameters of AWG10.

Parameter	R_0 (mΩ)	L_0 (μH)	C_0 (pF)
AWG10-9 m	64	4.49	281
Per unit length of AWG10	7.11	0.49	30.22

2.3. Simulation of influencing factors of voltage reflection

In order to verify that the influencing factors of voltage reflections in Section 2.2 includes length of the cable and the rise time of PWM pulse, a simulation model of the voltage reflection is built in the Simulink Module of Matlab. The cable lengths are selected as 10 m, 50 m and 100 m respectively. The simulation results are shown in Fig. 6. It can be seen that the cable length is proportional to the motor terminal voltage, which confirms to formula (6). When the length of the cable is less than 100 m, the amplitude of the motor terminal voltage increases greatly with the increase of the cable length. When the cable length is 10 m, the voltage peak value of the motor terminal is 452 V, and when the cable length is 100 m, the voltage peak value of motor terminal is 773 V.

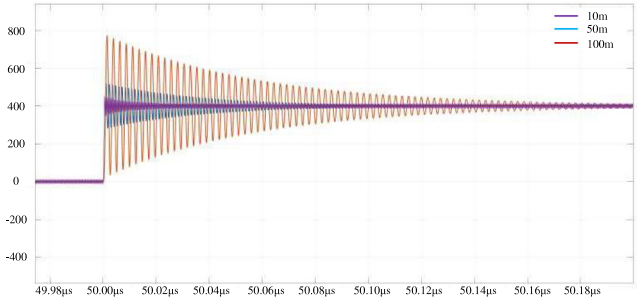

Fig. 6. Voltage reflection at the load terminal with different cable lengths.

The rise time of PWM pulse is selected as 100 ns, 500 ns and 1 μs respectively, and the simulation results are shown in Fig. 7. It can be seen that as the rise time increases, the amplitude of the motor terminal voltage is greatly reduced, which confirms to formula (6). When the pulse voltage rise time is 100 ns, voltage peak value of the motor terminal is 769 V, and when the pulse voltage rise time is 1 μs, the motor terminal voltage peak value is 416 V.

It can be seen that if the long cable has a fixed length, the best way is to reduce the rise time of the PWM pulse. However, if the switching speed of the SiC MOSFET is reduced, it will impact the power density of the motor drive system, and cannot make full potential of SiC MOSFET, so it is not considered.

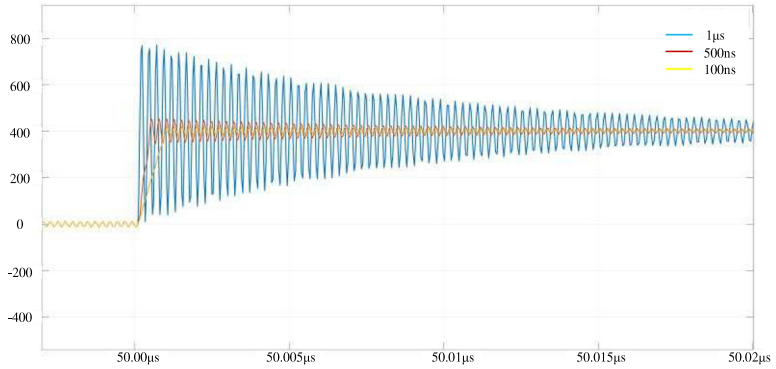

Fig. 7. Voltage reflection at the load terminal with different rise times of PWM pulse.

3. Passive *LRC* filter design

In order to reduce the voltage reflection problem, a suppression device can be added to the circuit. The *LRC* filter works by slowing down the t_r and t_f of the PWM pulse to reduce the du/dt of the output PWM.

Due to the symmetry of the three-phase system, one phase can be taken for analysis, and the equivalent circuit of one-phase of the inverter adding *LRC* filter is shown in Fig. 8. The *LRC* filter consists of an inductor L_f, a capacitor C_f and a resistor R_f. L_f and C_f form a series resonant circuit, and R_f and C_f are connected in series to adjust the loss.

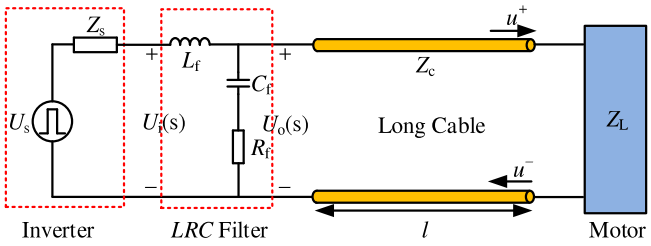

Fig. 8. Equivalent circuit of motor drive system with *LRC* filter.

The working principle of *LRC* is changing the input impedance at the end of the long cable. The *LRC* filter's response curve is relatively flat before the cutoff frequency ω_c, but drops sharply after the cutoff frequency, which has a good inhibitory effect on high-frequency components. The transfer function of the *LRC* filter is described as:

$$H(s) = \frac{\frac{R_f}{L_f}s + \frac{1}{L_f C_f}}{s^2 + \frac{R_f}{L_f}s + \frac{1}{L_f C_f}} = \frac{2\zeta\omega_n s + \omega_n^2}{s^2 + 2\zeta\omega_n s + \omega_n^2} \tag{7}$$

In order to completely suppress the overvoltage, the damping ratio ζ should not be less than 1, and the C_f is approximately short-circuit at high frequency. At the same time, in order to ensure that overvoltage of the motor occurs only once to reduce the energy consumption caused by voltage reflection, the R_f should be equal to the characteristic impedance Z_C of the cable. According to Shannon's sampling theorem, the high-frequency components with the oscillation period lower than $2t_{r\_c}$ should not be passed. So the frequency characteristics of the filter can be deduced:

$$H(j\omega) = \frac{U_o(j\omega)}{U_i(j\omega)} = \frac{jR_f C_f \omega + 1}{-L_f C_f \omega^2 + jR_f C_f \omega + 1} \tag{8}$$

In summary, we can design the *LRC* filter depending on the high-frequency parameters of the long cable which were extracted in Section 2 ($L_0 = 0.49$ μH/m, $R_0 = 4.24$ mΩ/m, $R_0 = 30.22$ pF/m). The cut-off angular frequency $\omega_c = 4.137 \times 106$ rad/s. The selected parameters of the filter are shown in Table 2.

Table 2. Parameters of the *LRC* filter.

Parameter	R_f (Ω)	L_f (μH)	C_f (nF)
Value	210	50	4.5

4. Experimental verification and discussion of voltage reflection suppression method

4.1. Experimental platform setup and testing principle

In order to explore the voltage reflection phenomenon under long cables, a voltage reflection test platform was established, as shown in Fig. 9. The power module adopts the 1200V/134A BSM120D12P2C005 SiC module from Rohm. The experimental cable is the 9 m-cable mentioned in 2.3. The experimental instruments includes the oscilloscope (DP0-2024B) from Tektronix, the rogowski coil (SS-282A) for measuring drain current, differential probe (SRS2100) for measuring load voltage U_L across load inductor and reverse voltage U_D of diode, and common probe(TPP0200) for measuring driving voltage.

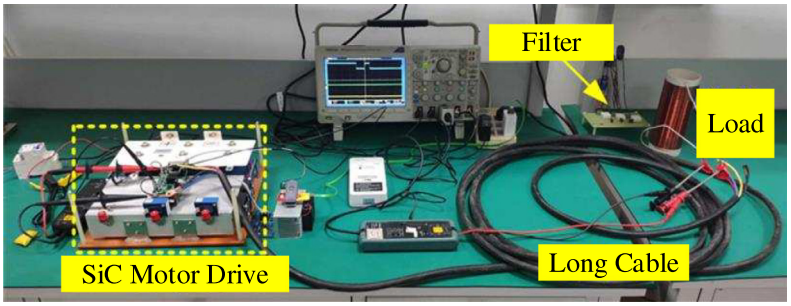

Fig. 9. Experimental platform setup of voltage reflection.

Fig. 10(a) shows the schematic diagram of the voltage reflection experiment. A long cable is connected between the diode and the inductor of the double-pulse test circuit. The test sequence used in the experiment is shown in Fig. 10(b), in which the first pulse for Q_L in the test sequence is generally used to establish the required test current I, and the second pulse is used to establish the required PWM pulse.

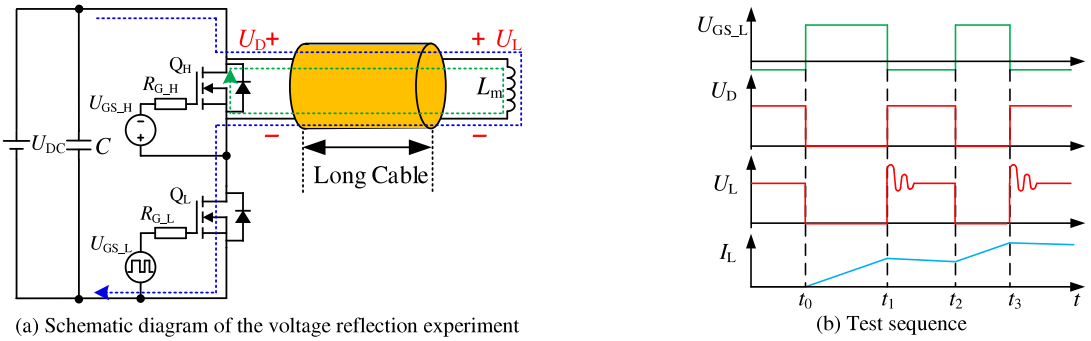

(a) Schematic diagram of the voltage reflection experiment

(b) Test sequence

Fig. 10. Voltage Reflection Test Process.

The specific working principle is as follows.

Stage 1 [$0 < t < t_1$]: At t_0, the driving voltage U_{GS_L} of Q_L becomes high, and the Q_L is turned on, the bus voltage U_{DC} is applied to both ends of the load inductance L_m, and the load current I_L rises linearly.

Stage 2 [$t_1 < t < t_2$]: At t_1, the Q_L is turned off. I_L freewheels through the upper tube D_H. The losses created in the diode cause the current to drop slightly. Until t_2, the driving voltage U_{GS_L} of the Q_L becomes high again.

Stage 3 [t_2 <t< t_3]: At t_2, the Q_L is turned on again, the required PWM pulse is set on the terminal of the load, and the waveforms of U_D an U_L can be obtained.

Stage 4 [t_3 <t< t_4]: At t_3, the Q_L is turned off again, the test experiment is finished.

4.2. Results and discussion

The voltage reflections without suppressing measures are tested when U_{DC} was 200 V and 400 V respectively, and voltage across the diode U_D and voltage across the load inductance U_L are obtained as shown in Fig. 11. When $U_{DC} = 200$ V, U_D is up to 224 V, and the peak value of U_L is 452 V, and the U_L is nearly twice as high as the U_D; When $U_{DC} = 400$ V, U_L is up to 432 V, and the peak value of U_L is 826 V, and the U_L is also nearly twice as high as the U_D. It can be seen that the impedance mismatch under the long cable condition will almost cause the voltage at the load double, affecting the insulation safety of the load inductance coil.

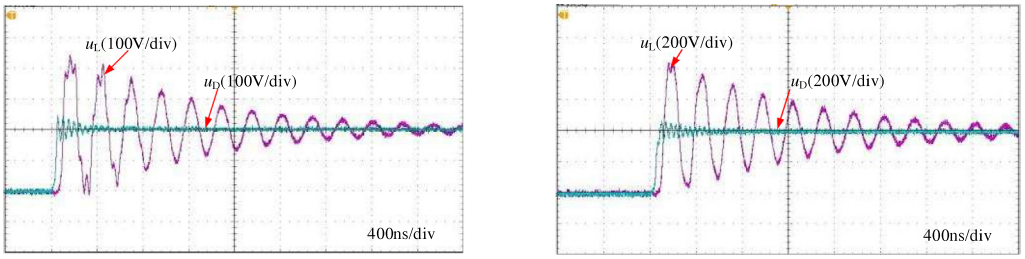

(a) Voltage reflection at U_{DC} = 200V (b) Voltage reflection at U_{DC} = 400V

Fig. 11. Voltage reflection without the *LRC* filter at different U_{DC}.

After connecting the designed *LRC* filter between the diode and the long cable, the voltage waveforms of the U_D and U_L are obtained as shown in Fig. 12. The peak value of the U_L dropped to 272 V at $U_{DC} = 200$ V, and only 524 V at $U_{DC} = 400$ V, so the effect of suppression method is obvious. At the same time, it can be found that after the filter is added, a delay of about 400 ns will occur at PWM pulse. Lower overshoot can be obtained, but at the expense of longer delay time. Therefore, the trade-off should be made in the choice of the filter parameters.

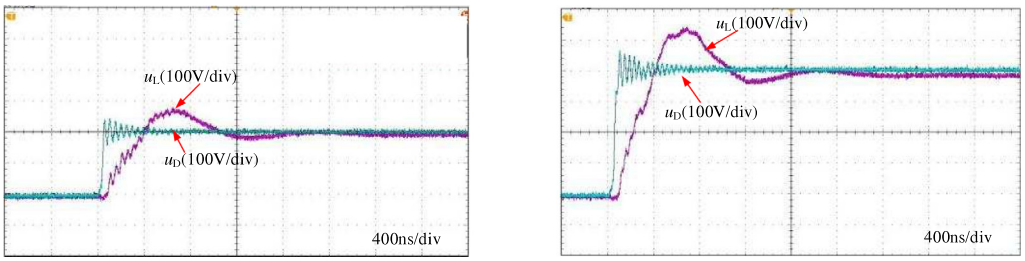

(a) Voltage reflection with the filter at U_{DC} = 200V (b) Voltage reflection with the filter at U_{DC} = 400V

Fig. 12. Voltage reflection with the *LRC* filter at different U_{DC}.

The waveforms of the line voltage at the motor with the *LRC* filter and without *LRC* filter are shown in Fig. 13. After the filter is connected, the line voltage is very clean with no obvious overshoot, and the peak value drops to about the bus voltage, indicating that the designed filter can effectively suppress the overvoltage problem at the motor.

5. Conclusions

In this paper, the principle and influencing factors of the voltage reflection caused by the long cable connected between the SiC-based motor drive system and the motor are analyzed, and the method of using the *LRC* filter to suppress the voltage reflection is proposed. The following conclusions may be drawn:

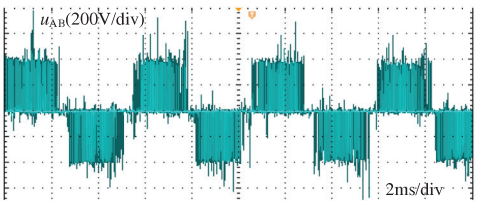

(b) Line voltage at the motor without the *LRC* filter

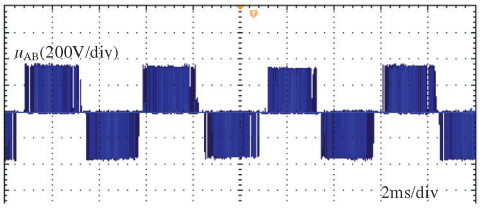

(a) Line voltage at the motor with the *LRC* filter

Fig. 13. Voltage reflection on the motor without *LRC* filter and with the filter.

(1) The amplitude of the overvoltage at the motor is affected by the length of the long cable and the switching speed of the SiC MOSFET, and as the cables becomes longer, or the switching speed becomes faster, the voltage reflection become more serious.

(2) By building the high-frequency model of the long cable, and exactly extracting the high-frequency impedance of the cable, the detailed design method of *LRC* filter and design process is put forward.

(3) The effect of the filter is verified on the voltage reflection test platform: when $U_{DC} = 200$ V and 400 V, the suppression degree is around 39.8% and 36.6% compared with the conditions without filter, and the line voltage at the motor driver is very clean, which means excellent suppression effect.

Declaration of competing interest

The authors declare that they have no known competing financial interests or personal relationships that could have appeared to influence the work reported in this paper.

Data availability

No data was used for the research described in the article.

Acknowledgment

This paper is supported financially in part by Zhejiang Science and Technology Project, China under grant Number LGG21E070001, State Key Laboratory of Wide-Bandgap Semiconductor Power Electronic Devices, China, under Grant Number 2019KF001 and in part by National Natural Science Foundation of China under grant Number 51677089.

References

[1] Morya AK, et al. Wide bandgap devices in ac electric drives: Opportunities and challenges. IEEE Trans Transp Electr 2019;5(1):3–20.
[2] Wang J, Veliadis V, Zhang J, Alsmadi Y, Wilson PR, Scott MJ. IEEE ITRW working group position paper-system integration and application: Silicon carbide: A roadmap for silicon carbide adoption in power conversion applications. IEEE Power Electr Mag 2018;5(2):40–4.
[3] Strom J, Korhonen J, Tyster J, Silventoinen P. Active du/dt–new output-filtering approach for inverter-fed electric drives. IEEE Trans Ind Electron 2018;58(9):3840–7.
[4] Velander E, et al. An ultralow loss inductorless dv/dt filter concept for medium-power voltage source motor drive converters with SiC devices. IEEE Trans Power Electr 2018;33(7):6072–81.
[5] De Caro S, et al. Motor overvoltage mitigation on SiC MOSFET drives exploiting an open-end winding configuration. IEEE Trans Power Electr 2019;34(11):11128–38.
[6] Ganesan N, Tallam R. Determination of cable characteristics and adjustment of PWM pulse pattern to minimize AC motor terminal over-voltage[c]. In: 2019 IEEE Applied power electronics conference and exposition. 2019, p. 1037–45.
[7] Diab MS, Yuan X. A quasi-three-level PWM scheme to combat motor overvoltage in SiC-based single-phase drives. IEEE Trans Power Electr 2020;35(12):12639–45.
[8] Zhang Y, Li H, Peng FZ. A low-loss compact reflected wave canceller for SiC motor drives. IEEE Trans Power Electron 2021;35(3):2461–5.

[9] Zhang Y, Li H. A WBG based active reflected wave canceller for SiC motor drives[c]. In: 2019 IEEE 7th Workshop on wide bandgap power devices and applications. 2019, p. 75–9.
[10] He J, et al. Multi-domain design optimization of dv/dt filter for SiC-based three-phase inverters in high-frequency motor-drive applications. IEEE Trans Ind Appl 2019;55(5):5214–22.
[11] Lee SangCheol, Nam KwangHee. Overvoltage suppression filter design methods based on voltage reflection theory. IEEE Trans Power Electr 2004;19(2):264–71.